RSC Advances

PAPER

View Article Online
View Journal | View Issue

Cite this: *RSC Adv.*, 2026, **16**, 29470

Design and evaluation of a thiazoline-appended imidazole based fluorescent turn on chemosensor for Hg^{2+} ion detection: spectroscopic characterization and solid state film applications

Bharathkumar Thangaraj,[a] Suresh Ranganathan,[bc] Ravichandran Cingaram,[a] Lakshmipriya Kannan,[a] Sathiyanarayanan Kulathu Iyer[d] and Karthikeyan Natesan Sundaramurthy *[a]

Mercury contamination presents a significant environmental and biological hazard, necessitating the development of reliable and sensitive fluorescent probes for the detection and removal of mercury ions. In this study, a novel fluorogenic chemosensor (BTA) incorporating a sulfur- and nitrogen-donor analogue of 4-(bis(2-((4,5-dihydrothiazol-2-yl)thio)ethyl)amino)benzaldehyde, has been synthesized for the selective detection of Hg^{2+} ions. BTA exhibits excellent chemo-selectivity and high sensitivity towards Hg^{2+} ions in a binary mixture of acetonitrile–water medium ($CH_3CN : H_2O$) (6 : 4, v/v), showing a distinct red shift (~15 nm) in absorption spectrum and a pronounced fluorescence "turn-on" response. The detection limit was determined to be 114.7 nM, confirming its superior analytical performance. Detailed spectroscopic investigations, including Job's plot, proton NMR titration, HR-MS, FT-IR, and DFT calculations, confirm a 1 : 1 binding stoichiometry between BTA and Hg^{2+}. The probe displays a prompt emission response, excellent reversibility, and strong anti-interference capability. Moreover, a Boolean logic gate (AND) was developed using the emission response of BTA to achieve selective detection of Hg^{2+} ions. Furthermore, a BTA infused PVA solid-state fluorescent film (BTA/PVA) was developed, enabling efficient recognition of deadly Hg^{2+} under practical conditions.

Received 9th April 2026
Accepted 26th May 2026

DOI: 10.1039/d6ra03004a

rsc.li/rsc-advances

Introduction

Mercury poisoning remains a severe environmental and health problem, owing to its persistence, extreme toxicity, and bioaccumulative tendency, even at minimum concentration. The divalent mercury ions (Hg^{2+}) are predominantly hazardous because it quickly binds with sulfur and nitrogen-containing biomolecules, causing protein denaturation and disruption of enzymatic and neuronal activities.[1–3] Exposure to Hg^{2+} has been connected with vital physiological processes, resulting in severe disorders such as neurotoxicity, nephrotoxicity, hepatotoxicity, and developmental abnormalities, stressing the crucial need for effective and rapid detection methods.[4–7]

Various advanced analytical instrumentation techniques, including atomic absorption spectroscopy (AAS),[8] anodic stripping voltammetry (ASV),[9] γ-ray spectrometry,[10] inductively coupled plasma mass spectrometry (ICP-MS)[11] and electrophoresis[12] have been used for mercury detection. Although these methods provide outstanding precision and sensitivity, their practical value is limited by expensive instrumentation, trained operators, time-consuming sample preparation, and lack of portability, rendering them unsuitable for routine or on-site detection.[13,14] Therefore, the development of facile, cost-effective, and rapid sensing approaches capable of detecting Hg^{2+} ions with high sensitivity and selectivity under ambient conditions remains an important goal.[15–17] As a result, fluorescent chemical sensors have materialized as powerful substitutes due to their high sensitivity, operational simplicity, fast response time, with potential visual detection.[18] Various organic chemoprobes, including rhodamine,[19] BODIPY,[20] coumarin,[21] phenanthridine,[22] triphenylamine (TPA),[23] imidazole,[24] Schiff's base[25] and thiazoline derivatives have been exploited for mercury sensing through diverse mechanisms such as photo-induced electron transfer (PET), aggregation-induced emission (AIE), metal-induced fluorescence enhancement or quenching and intramolecular charge transfer (ICT).[26,27] However, our study focuses on imidazole-based probes, as several previously documented probes suffer from drawbacks, such as turn-off

[a]*Department of Chemistry, Easwari Engineering College, Chennai, India. E-mail: karthikeyan.ns12@gmail.com*

[b]*Department of Chemistry, Karpagam Academy of Higher Education, Coimbatore, India*

[c]*Centre for Material Chemistry, Karpagam Academy of Higher Education, Coimbatore, India*

[d]*Chemistry Division, School of Advanced Sciences, Vellore Institute of Technology, Chennai, India*

responses, solvent dependence, and exhibits poor performance.[28–32] In contrast, the probe BTA displays a fluorescence "turn-on" response to Hg^{2+} with high sensitivity and selectivity. Moreover, its successful integration of BTA into PVA addressing key constraints of previous methods.

In this work, we report the design and synthesis of a novel sulfur- and nitrogen-rich fluorogenic probe (BTA), derived from the reaction of 4-(bis(2-((4,5-dihydrothiazol-2-yl)thio)ethyl) amino)benzaldehyde and benzil. The probe exhibits pronounced selectivity and sensitivity toward Hg^{2+} ions in an aqueous acetonitrile medium, accompanied by an intense fluorescence enhancement. In addition, BTA integrated poly(-vinyl alcohol) (PVA) matrix yields a fluorescence ON robust solid-state film sensor capable of selective detection of Hg^{2+} ions, offering a promising strategy for practical, on-site mercury monitoring applications.[33]

Experimental section

Reagents and instruments

Unless otherwise specified, all reagents and solvents were obtained from commercial suppliers and used without further purification. Thin-layer chromatography (TLC) was performed on silica gel 60 F^{254} plates to monitor reaction progress. ^{1}H NMR and ^{13}C NMR spectra of BTA were recorded on a Bruker 400 MHz spectrometer using tetramethylsilane (TMS) as an internal reference, and chemical shifts (δ) are reported in parts per million (ppm). FT-IR spectra were recorded on a JASCO-4100. High-resolution mass spectrometry data were obtained using a WATERS XEVO G2-XS QToF mass spectrometer. UV-visible absorption spectra were recorded on a JASCO V-750 spectrophotometer, while emission spectra were obtained using a JASCO FP-8300 spectrofluorometer at ambient temperature. All metal ion stock solutions were freshly prepared for analytical measurements using deionized water.

Preparation of stock and working solutions

BTA was dissolved in an acetonitrile–water mixture (CH_3CN : H_2O = 6 : 4, v/v) to prepare a 1 mM stock solution, which was subsequently diluted to 20 μM for UV-visible and fluorescence spectroscopic studies. Solutions of various ions, including Hg^{2+}, Ni^{2+}, Na^+, Mo^{6+}, Li^+, Mn^{2+}, Mg^{2+}, K^+, Fe^{2+}, Cd^{2+}, Ca^{2+}, Zn^{2+} Co^{2+}, Ba^{2+}, Ag^+, Sr^{2+}, W^{6+}, Br^-, Cl^-, CN^-, F^-, HS^-, I^-, SCN^-, NO_2^-, $H_2PO_4^-$, HSO_4^-, and NO_3^- ions were prepared at 1 mM concentrations in deionized water and used as analytes. The excitation wavelength for emission measurements was set at 325 nm, and all spectral experiments were carried out at room temperature using the same solvent composition (CH_3CN : H_2O = 6 : 4, v/v).

Synthesis of chemoprobe BTA

The synthetic pathway for chemoprobe BTA is illustrated in Scheme 1. The 2 TA was obtained using a method adapted from a previously published procedure.[4] Briefly, benzil (0.12 g), 2 TA (0.3 g), and ammonium acetate (0.45 g) were dissolved in 25 mL of glacial acetic acid (AcOH) and the reaction mixture was refluxed for 6 h with constant stirring. The completion of reaction was monitored by TLC method, then the mixture was cool to ambient temperature, and extracted three times with chloroform (3 × 30 mL). The organic layers were dried over anhyd. $NaSO_4$, and concentrated under reduced pressure. The crude residue was purified by column chromatography using hexane/ethyl acetate (6 : 4 v/v) solvent system. The desired compound (BTA), was obtained as a yellow solid in 75% yield. The structure of BTA was confirmed by ^{1}H NMR, ^{13}C NMR, FT-IR, and HR-MS analyses (Fig. S3–S6). ^{1}H NMR (400 MHz, DMSO-d_6), δ (ppm): 12.35 (1H), 7.92–7.90 (2H), 7.53–7.35 (10H), 7.05–7.03 (2H) 4.26–4.22 (4H), 3.68–3.65 (4H), 3.52–3.48 (4H), 3.30–3.26 (4H); ^{13}C NMR (100 MHz, DMSO-d_6) 172.48, 163.61, 147.43, 146.83, 128.83, 127.04, 119.05, 112.13, 64.48, 50.16, 35.84, 29.47, 21.52. IR: 2916 cm^{-1}, 1566 cm^{-1}, 1496 cm^{-1}, 1284 cm^{-1}, 1134 cm^{-1}, 956 cm^{-1}, 690 cm^{-1}, and; HR-MS for $C_{31}H_{31}N_5S_4$ calc. $[M]^+$ m/z, 601.1462; experimental value $[M + H]^+$ m/z, 602.1542.

Results and discussion

Spectroscopic insights into the sensing performance of BTA

The sensing features of the newly designed chemoprobe BTA were systematically examined to evaluate its selectivity and sensitivity towards diverse metal ions. To assess its sensing property, both UV-visible and fluorescence spectroscopy were

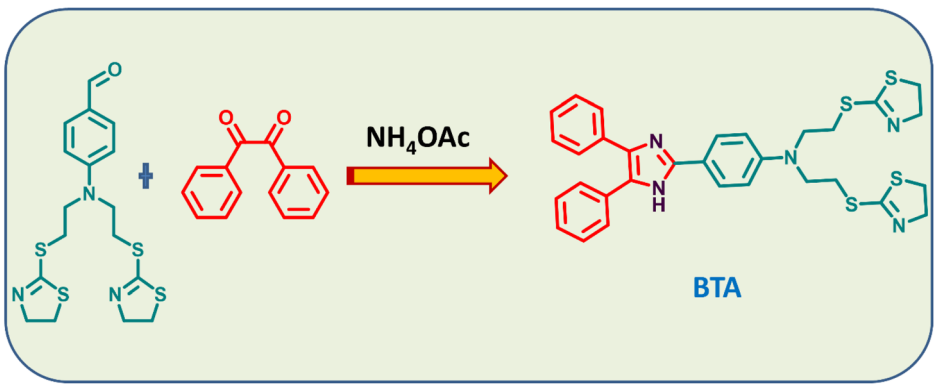

Scheme 1 Schematic representation for synthesis of probe BTA.

performed in the presence of series metal cations and anions, including Hg^{2+}, Ni^{2+}, Na^{+}, Mo^{6+}, Li^{+}, Mn^{2+}, Mg^{2+}, K^{+}, Fe^{2+}, Cd^{2+}, Ca^{2+}, Zn^{2+} Co^{2+}, Ba^{2+}, Ag^{+}, Sr^{2+}, W^{6+}, Br^{-}, Cl^{-}, CN^{-}, F^{-}, HS^{-}, I^{-}, SCN^{-}, NO_2^{-}, $H_2PO_4^{-}$, HSO_4^{-}, and NO_3^{-} ions. All spectroscopic measurements were studied in a mixed solvent system of acetonitrile and water ($CH_3CN : H_2O = 6 : 4$, v/v) mixture.

In the absorption spectrum the probe BTA exhibited a prominent red shift (~15 nm) exclusively for Hg^{2+} ions, while other tested cations (Fig. 1a) and anions (Fig. S7) induce negligible changes, suggesting a target specific recognition. These observations clearly validate the selective recognition of Hg^{2+} ions by probe BTA, whereas other cations (Fig. 1b) and anions (Fig. S7b) failed to produce any comparable fluorescence variations (Fig. 1f). To acquire deeper understanding into the interaction mechanism, UV-vis titration experiments were performed by gradually increasing the concentration of Hg^{2+} ions. The absorbance spectrum of BTA exhibited an intense absorption band centered at 325 nm, which progressively decreased in intensity with increasing concentration of Hg^{2+} ions. Simultaneously, a new absorption band appeared at 340 nm, accompanied by the emergence of an isosbestic point at 335 nm (Fig. 1c). The presence of the isosbestic point indicates a well-

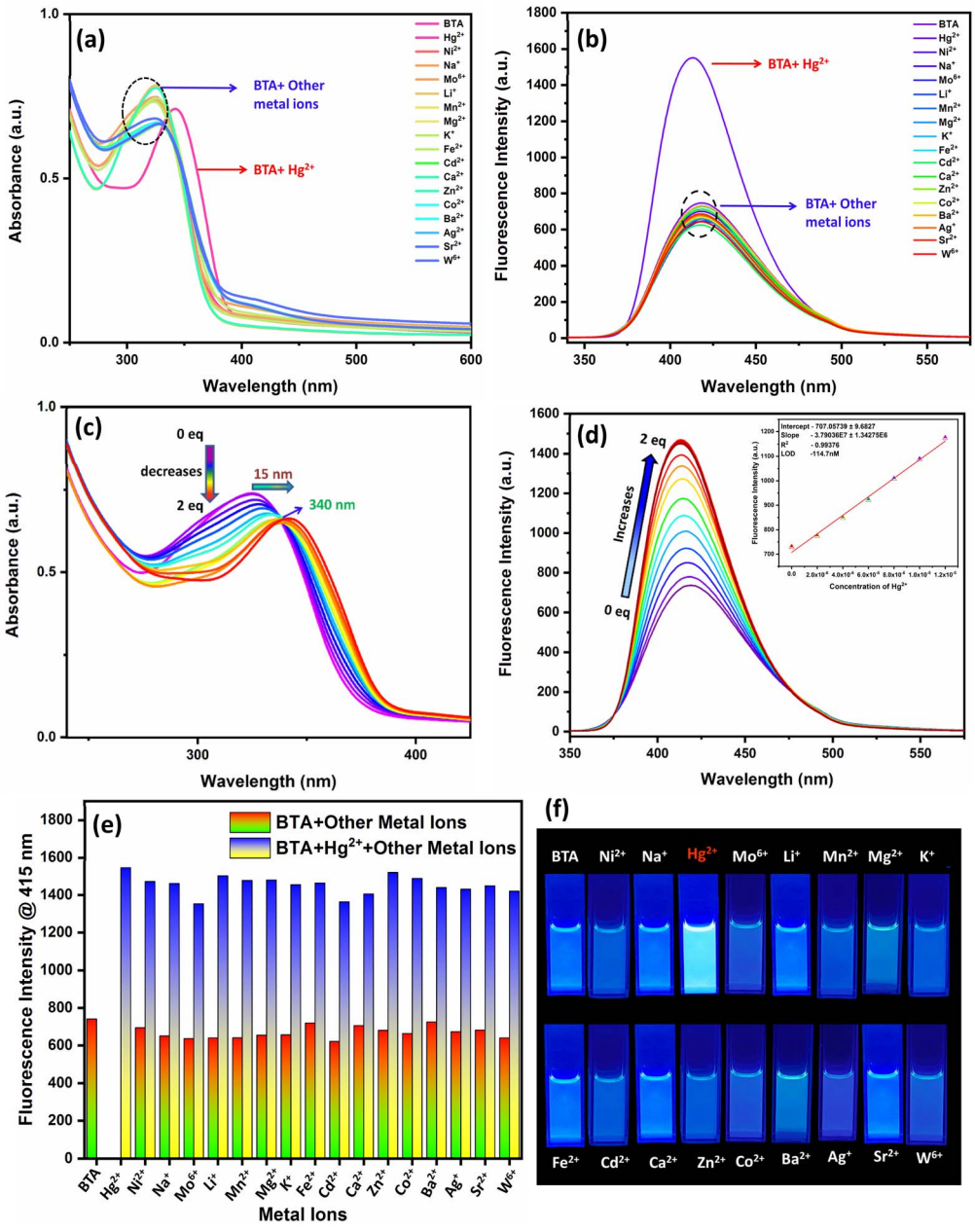

Fig. 1 (a) UV-vis absorption spectra and (b) fluorescence spectra of probe BTA (20 μM) in ($CH_3CN : H_2O$) (6 : 4, v/v) solution in response to 1 mM of diverse metal cations (5 equiv.). Variation of (c) UV-vis absorption spectra and (d) emission spectra of probe BTA in the presence of increasing concentration of Hg^{2+} ions (0–2 equiv.) inset: linear response curve of BTA depending on the various concentration of Hg^{2+} ions. (e) Competition experiments of BMA (20 μM) toward Hg^{2+} ions in the presence of 10 mM of other metal ions in CH_3CN/H_2O (6 : 4, v/v). (f) Photograph of probe BTA before and after addition of metal ions under UV region.

defined equilibrium between the BTA and BTA–Hg^{2+} complex. Fluorescence titration experiments provided further evidence for this interaction. As presented in Fig. 1d, a substantial enhancement in emission intensity at 418 nm was observed upon the progressive addition of Hg^{2+} ions (Fig. S8), reaching saturation after the introduction of one equivalent of Hg^{2+} ions. The other metal ions did not induce any notable emission responses, highlighting its excellent specificity of probe BTA towards Hg^{2+} ions. The linear relationship between fluorescence intensity and Hg^{2+} concentration exhibited an excellent correlation ($R^2 = 0.99529$), from which the detection limit was estimated to be 114 nM, demonstrating the high sensitivity of BTA for Hg^{2+} ions detection. The observed enhancement in emission intensity can be attributed to the restriction of photo induced electron transfer (PET) or suppression of non-radiative decay processes upon coordination with Hg^{2+}.[34]

The fluorescence quantum yield was determined using anthracene as a reference with a known ϕ_R of 0.27 in ethanol. The calculated quantum yield values were 0.022 for BTA, and 0.043 for BTA–Hg^{2+} complex. These results clearly indicate an enhancement in fluorescence intensity upon binding of BTA with Hg^{2+} ions.

To confirm the anti-interference capability of probe, competitive fluorescence studies were performed in the presence of different coexisting metal cations (Fig. 1e and S9a) and mixed ions (Fig. S9b). The emission response of BTA to Hg^{2+} remained unaffected, even under competitive conditions, confirming its robust selectivity. Collectively, these results demonstrate that BTA severs as a highly selective and sensitive fluorescent ON chemoprobe for the detection of Hg^{2+} ions with clear optical transitions and strong resistance towards various interfering metal species in a mixed solvent system.

Elucidation of binding stoichiometry and sensing mechanism of BTA

Based on the spectroscopic outcomes, the plausible sensing mechanism for the coordination of probe BTA to Hg^{2+} is proposed. Upon coordination with Hg^{2+} ions, probe BTA displays a fluorescence turn-on signal owing to target specific interaction of Hg^{2+} with the donors of nitrogen and sulfur atoms present in 4-(bis(2-((4,5-dihydrothiazol-2-yl)thio)ethyl) amino)benzaldehyde moiety.

To validate this proposed sensing mechanism, Job plot, NMR titration, FT-IR and HR-MS studies were systematically performed. The Job's plot analysis revealed the formation of a 1 : 1 binding stoichiometric adduct between BTA and Hg^{2+} (Fig. S10). This observation was further corroborated by HR-MS analysis (Fig. S11). In the mass spectrum the peak at m/z value of 839.5945 corresponding to [BTA + Hg^{2+} + $2H_2O$], corroborating the proposed complexation stoichiometry. The K_d value for Hg(II) was 5.4 nM ($R^2 = 0.99$) (Fig. S12).

To acquire deeper insight into the binding interaction, ^{1}H NMR titration experiment was performed in DMSO-d_6 solvent. Fig. 2 displays the configurations of protons in BTA after interaction with Hg^{2+} ions. The resonance signals observed in the region of 3.26–4.26 ppm correspond to the aliphatic protons of BTA. The proton signals at 7.03–7.05 (H_b) and 7.90–7.92 (H_c) ppm are assigned to the aromatic protons of binding unit. While the biphenyl aromatic protons appear as merged signals

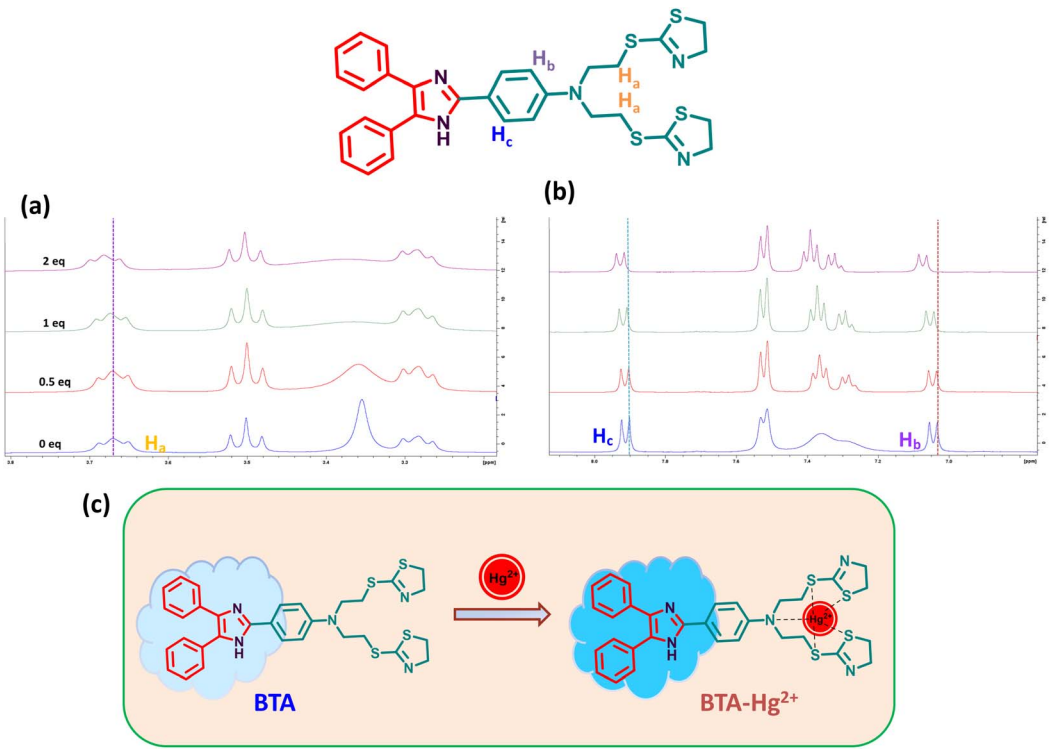

Fig. 2 ^{1}H NMR titration of probe BTA with Hg^{2+} (0–2 eq.) in DMSO-d_6. (a) Aliphatic region; (b) aromatic region. (c) Proposed reaction mechanism for probe BTA with Hg^{2+} ions.

at 7.56–7.22 ppm. Nevertheless, following addition of Hg^{2+} ions, the peak of H_a proton at the aliphatic region undergoes a slight shift from 3.66–3.68 ppm. Due to the geometrical coordination the aromatic protons of and H_b and H_c a small downfield shift to 7.91–7.94 ppm and 7.06–7.08 ppm. Furthermore, the biphenyl aromatic proton signals at the region 7.55–7.28 ppm displayed clear splitting. These spectral perturbations strongly suggest that the nitrogen and sulfur atoms of the thiazoline moiety and the nitrogen on the phenylamine serve as the primary binding sites for Hg^{2+} ions.

The FT-IR spectra of BTA in the absence and presence of Hg^{2+} were recorded and are shown in Fig. S13. For BTA, the absorption bands observed at 956, 1134, 1284, and 1566 cm^{-1} correspond to C–C stretching, C–N stretching, C–N (ring stretching), and C=N stretching, respectively. Upon coordination with Hg^{2+}, the FT-IR spectrum of BTA–Hg^{2+} exhibits significant band broadening and partial merging of these characteristic vibrations, particularly in the C–N/C–C regions, while the C=N stretching band disappears. These spectral changes indicate a strong interaction between Hg^{2+} ions and the receptor unit of BTA, confirming the involvement of heteroatoms in metal coordination (Fig. 2c).

Evaluation of the reversible, kinetic, and logical sensing functions of BTA

Reversibility is an important criterion for estimating the practical applicability of a fluorescent sensor. The reversible sensing behaviour of the probe BTA to Hg^{2+} ions were studied in a binary solvent system ($CH_3CN : H_2O = 6 : 4$, v/v) using KI as a regenerating agent. The probe BTA displayed nominal emission centered at 413 nm. Upon interacting with Hg^{2+} ions, the emission intensity increased at 418 nm, indicating complex formation between BTA and Hg^{2+} ions, following addition of potassium iodide (KI) decreased the fluorescence to the original level of BTA signal (Video S1), which confirms the restoration of free probe BTA.

Upon alternative addition of Hg^{2+} and KI demonstrated a clear OFF–ON–OFF switching pattern of the reversible fluorescence phenomenon. The fluorescence response remained constant over five successive cycles, demonstrating the repeatability of the probe BTA (Fig. 3a). These observations confirm the excellent reversibility and regeneration capability of BTA, an essential attribute for reusable sensing applications.

To further authenticate the sensing performance, the response kinetics of BTA towards Hg^{2+} ions were examined using time-resolved fluorescence spectroscopy. Time-dependent fluorescence measurements showed that the emission intensity at 418 nm of BTA reached its maximum within 4 seconds after the addition of Hg^{2+} (Video S2), after which it remained constant without further variation in emission intensity. This rapid response towards Hg^{2+} ions, demonstrates its potential for real-time monitoring of mercury contamination (Fig. 3b).

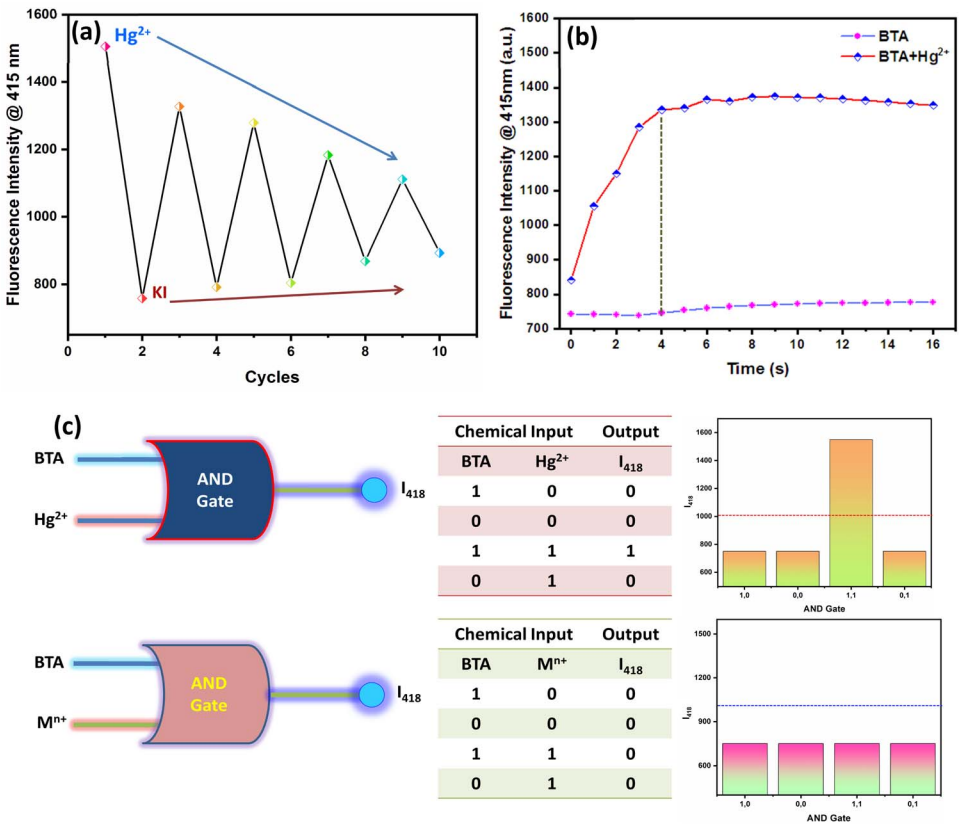

Fig. 3 (a) Change in fluorescence of BTA after the sequential addition of Hg^{2+} and KI. (b) The time-dependent fluorescence spectra of BTA–Hg^{2+} complex. (c) Logic representation of molecular AND gate; Truth table of AND gate; bar diagram of AND gate for Hg^{2+} ions and other metal ions.

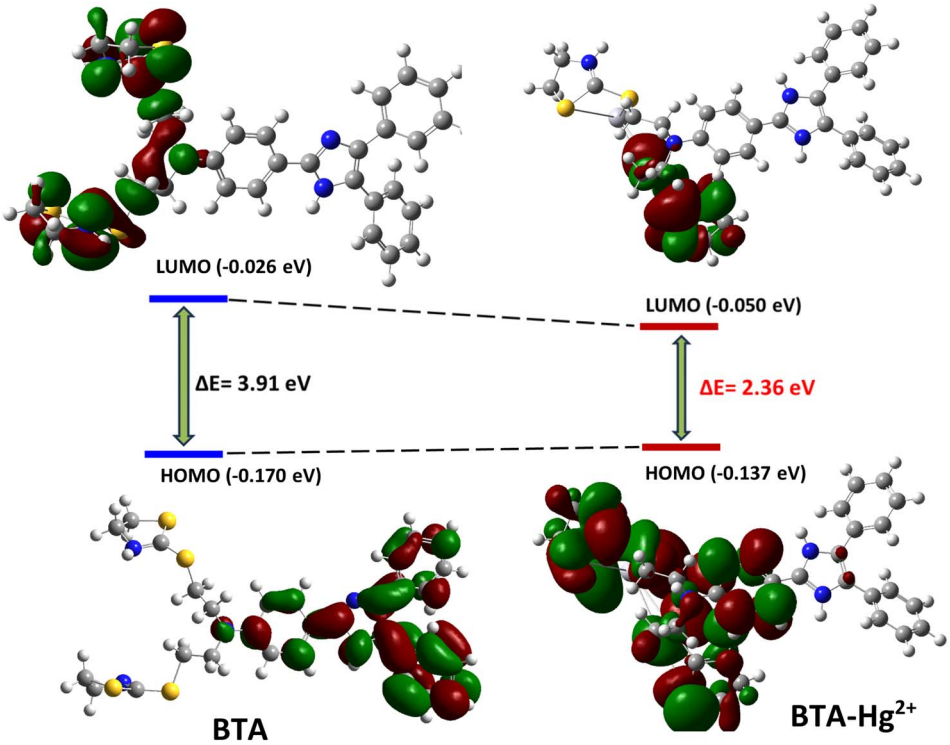

Fig. 4 Frontier molecular orbital (FMOs) of the BTA and the BTA–Hg^{2+} complex.

In addition to its reversible and rapid response characteristics, this system was also explored for its molecular logic gate functionality. Inspired by the growing interest in molecular systems capable of mimicking digital operations, the fluorescence modulation of BTA was employed to design a molecular AND logic gate (Fig. 3c). In this logical framework, BTA, Hg^{2+}, and various metal ions (M^{+}) were assigned as chemical inputs, while the emission intensity at 418 nm (I_{418}) was assigned as the optical output. The output followed a binary threshold: I_{418} > 1000 corresponds to "1" (ON) and ≤1000 to "0" (OFF). Only when both BTA and Hg^{2+} were present, the system exhibits strong fluorescence, producing an output of "1," thus satisfying the AND gate logic. Other metal ions failed to activate fluorescence enhancement, yielding a "0" output corresponding to the OFF state.

Thus, the probe BTA efficiently functions as a molecular AND logic gate, combining selective Hg^{2+} recognition with an intelligent optical signal processing.

Quantum chemical investigations of BTA

To gain better insight into the photophysical behaviour of the probe BTA and its complex with Hg^{2+} ions, density functional theory (DFT) calculations were performed using Gaussian 09. Geometry optimizations of the free probe BTA were performed at the B3LYP/6-31G (d,p) level, whereas the B3LYP/LANL2DZ basis set was used for the BTA–Hg^{2+} complex. The Frontier Molecular Orbitals (FMOs) of BTA and its metal complex are displayed in Fig. 4. In the free BTA molecule, the HOMO electron density is primarily localized over the diphenyl unit and recognition moiety, while the LUMO electron density is located over the 2 thiazoline thiol parts. In contrast, for the BTA–Hg^{2+} complex, the electron density of HOMO was distributed over receptor region, but the LUMO becomes predominantly localized on Hg^{2+}. This redistribution of electron density upon Hg^{2+} coordination supports a photoinduced electron transfer (PET) mechanism as the basis of fluorescence enhancement.[35] The calculated HOMO–LUMO energy gaps for BTA and BTA–Hg^{2+} are 3.91 eV and 2.36 eV, respectively. The reduction in energy gap upon complexation indicates enhanced electronic delocalization and the formation of a more stable complex, which corroborates well with the experimentally observed fluorescence "ON" response of BTA toward Hg^{2+} ions.

Solid-state sensing application of BTA–PVA film

The development of solid-state sensing materials based on polymers has become important for environmental and biological monitoring, predominantly for the recognition of hazardous ions. Among such materials, polyvinyl alcohol (PVA) films have emerged as a best platform owing to their optical transparency, mechanical flexibility, chemical stability, and their capability to uniform immobilization of ligands.[36,37]

2 g of PVA was dissolved in 20 mL of deionized water and heated to 90 °C for 3 h to obtain a uniform solution. Once cooled to room temperature, 2 mL of BTA solution (0.02 g mL^{-1}) was introduced, followed by further stirring for 1 hour. The resulting solution was poured into a clean Petri dish and left to dry under ambient conditions for about 48 hours.[38] The dried BTA/PVA (2 wt%) film was then carefully peeled off and cut into

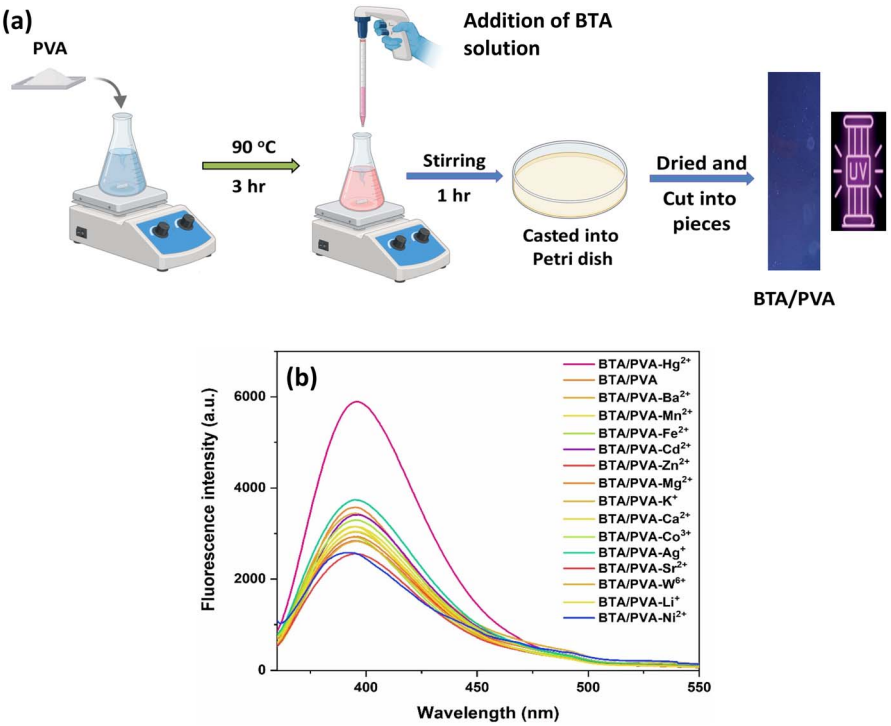

Fig. 5 (a) Fabrication of BTA/PVA film; (b) fluorescence spectra of solid-state detection of mercury ions using PVA/BTA.

the required shapes (Fig. 5a). The film exhibited weak blue fluorescence under UV region, making it suitable for the detection of Hg^{2+} ions *via* fluorescence "turn-on" response. The emission spectra exposed that, although the BTA/PVA film displayed moderate emission, a striking enhancement in fluorescence intensity at 395 nm was observed only for Hg^{2+} ions (Fig. 5b). On the other hand, only slight changes in emission intensity were observed for tested various cations, emphasizing the remarkable selectivity of the BTA/PVA film. In addition, a quantitative analysis for BTA/PVA film was carried out using Hg^{2+} ions, upon increasing the concentration of Hg^{2+} ions, the fluorescence intensity was increased progressively, which was correlated with the life time measurements (Fig S15). The turn-on response toward Hg^{2+} ions is due to favourable binding interactions that restrict non-radiative decay.

Overall, this matrix-assisted emission enhancement, combined with the film's stability and simplicity, shows that BTA/PVA is a highly promising material for practical solid-state mercury monitoring applications.

Comparison with other chemosensors

The advanced sensing performance of the probe BTA was assessed with previously reported mercury sensors (Table S1). BTA displays several distinct advantages, such as noticeable fluorescence turn-on response, robust anti-interference ability, excellent reversible behaviour, and rapid reaction kinetics. Furthermore, the successful incorporation of BTA into PVA films demonstrates the possibility for practical and on-site mercury detection. Collectively, these features make BTA as a highly promising material for environmental monitoring and remediation applications.

Conclusion

In conclusion, by engineering an imidazole-based ligand, we developed a fluorescent chemosensor (BTA) for the selective and sensitive detection of Hg^{2+} ions. The chemoprobe BTA displayed a prominent emission enhancement upon interaction with Hg^{2+} ions, with the detection limit of 114 nM. The plausible binding mechanism between BTA and Hg^{2+} ions was systematically interpreted through UV-vis and fluorometric titrations, NMR spectroscopy, HR-MS, and FT-IR analysis, in addition DFT calculations provided theoretical authentication for the proposed sensing mechanism. Additionally, the practical applicability of the chemoprobe BTA was demonstrated by its successful utilization in PVA film-based detection, highlighting its potential for real-world environmental monitoring.

Author contributions

Bharathkumar Thangaraj: conceptualization, writing original draft; Suresh Ranganathan: data curation, methodology; Lakshmipriya Kannan: formal analysis, writing – review & editing; Karthikeyan Natesan Sundaramurthy: supervision, validation; Ravichandran Cingaram: project administration, resources; Sathiyanarayanan Kulathu Iyer: project administration, resources.

Conflicts of interest

There are no conflicts to declare.

Data availability

Data will be made available on request.

Supplementary information (SI): characterization data, photophysical studies, and additional spectra and figures supporting the findings of this work. See DOI: https://doi.org/10.1039/d6ra03004a.

Acknowledgements

NSK acknowledges the DST – SERB for Young Scientist Scheme Project (Ref. No. SB/FT/CS-067/201S), Atomic Energy Regulatory Board, India for sanctioning the CSRP project (Ref. No. AERB/CSRP/PROJ. No. 65/06/2017), and the Grand-in-Aid by FIST scheme from Department of Science and Technology, India (SR/FIST/college-110/2017).

References

1 L. T. Budnik and L. Casteleyn, *Sci. Total Environ.*, 2019, **654**, 720–734.
2 J. Hu, X. Yu, X. Zhang, C. Jing, T. Liu, X. Hu, S. Lu, K. Uvdal, H. W. Gao and Z. Hu, *Spectrochim. Acta, Part A*, 2020, **241**, 118657.
3 S. Zeng, S. J. Li, X. J. Sun, T. T. Liu and Z. Y. Xing, *Dyes Pigm.*, 2019, **170**, 107642.
4 B. Thangaraj, S. K. Iyer, R. Cingaram and K. N. Sundaramurthy, *J. Mater. Chem. C*, 2025, **13**, 15070–15081.
5 Y. S. Wu, A. I. Osman, M. Hosny, A. M. Elgarahy, A. S. Eltaweil, D. W. Rooney, Z. Chen, N. S. Rahim, M. Sekar, S. C. Gopinath and N. N. M. Rani, *ACS Omega*, 2024, **9**, 5100–5126.
6 S. Chakraborty, K. Das and S. Halder, *Inorg. Chim. Acta*, 2024, **566**, 122026.
7 H. Park, S. Subedi, E. T. Oh, H. J. Park and K. H. Lee, *Microchem. J.*, 2024, **200**, 110375.
8 W. R. Hatch and W. L. Ott, *Anal. Chem.*, 1968, **40**, 2085–2087.
9 H. Xiao, W. Wang, S. Pi, Y. Cheng and Q. Xie, *Sens. Actuators, B*, 2020, **317**, 128202.
10 A. Pantelica, I. I. Georgescu, M. D. Murariu-Magureanu, I. Margaritescu and E. Cincu, *Radiat. Prot. Dosim.*, 2001, **97**, 187–191.
11 E. A. Casartelli and N. Miekeley, *Anal. Bioanal. Chem.*, 2003, **377**, 58–64.
12 B. F. Liu, L. B. Liu and J. K. Cheng, *Talanta*, 1998, **47**, 291–299.
13 M. Sarkar, S. Banthia and A. Samanta, *Tetrahedron Lett.*, 2006, **47**, 7575–7578.
14 C. Yuan, S. Li, Y. Wu, L. Lu and M. Zhu, *Sens. Actuators, B*, 2017, **242**, 1035–1042.
15 M. D. Gholami, S. Manzhos, P. Sonar, G. A. Ayoko and E. L. Izake, *Analyst*, 2019, **144**, 4908–4916.
16 R. Ali, I. A. Ali, S. Messaoudi, F. M. Alminderej and S. M. Saleh, *J. Mol. Liq.*, 2021, **336**, 116122.
17 H. Park, E. T. Oh, J. Park, S. Subedi, H. J. Park and K. H. Lee, *Anal. Chem.*, 2025, **97**, 5982–5991.
18 P. K. Mehta, H. Park, E. T. Oh, H. J. Park and K. H. Lee, *Sens. Actuators, B*, 2023, **385**, 133670.
19 J. Mandal, P. Ghorai, K. Pal, T. Bhaumik, P. Karmakar and A. Saha, *ACS Omega*, 2019, **5**, 145–157.
20 A. V. Raveendran, P. A. Sankeerthana, A. Jayaraj and P. C. A. Swamy, *Results Chem.*, 2022, **4**, 100297.
21 D. Cao, Z. Liu, P. Verwilst, S. Koo, P. Jangjili, J. S. Kim and W. Lin, *Chem. Rev.*, 2019, **119**, 10403–10519.
22 B. Thangaraj, S. Baskaran, R. Cingaram, S. K. Iyer and K. N. Sundaramurthy, *Spectrochim. Acta, Part A*, 2025, **327**, 125312.
23 M. Ponram, B. Thangaraj, S. Ranganathan, B. Sambath, R. Cingaram, S. K. Iyer and K. N. Sundaramurthy, *Inorg. Chem. Commun.*, 2023, **157**, 111345.
24 G. Emandi, K. J. Flanagan and M. O. Senge, *Photochem. Photobiol. Sci.*, 2018, **17**, 1450–1461.
25 M. A. Alhamami, A. Y. Mohammed, J. S. Algethami, H. M. Al-Saidi, S. Khan and S. S. Alharthi, *Microchem. J.*, 2024, **197**, 109817.
26 S. Erdemir, M. Oguz and S. Malkondu, *Anal. Chim. Acta*, 2022, **1192**, 339353.
27 M. F. Arshad, A. Alam, A. A. Alshammari, M. B. Alhazza, I. M. Alzimam, M. A. Alam, G. Mustafa, M. S. Ansari, A. M. Alotaibi, A. A. Alotaibi and S. Kumar, *Molecules*, 2022, **27**, 3994.
28 B. Thangaraj, M. Ponram, S. Ranganathan, B. Sambath, R. Cingaram, S. K. Iyer and K. N. Sundaramurthy, *RSC Adv.*, 2023, **13**, 26023–26030.
29 S. M. Kumar, D. Jothi, S. Munusamy, S. Enbanathan and S. K. Iyer, *J. Photochem. Photobiol., A*, 2023, **434**, 114269.
30 S. M. Kumar, S. Munusamy, D. Jothi, S. Enbanathan, J. Haribabu and S. K. Iyer, *Opt. Mater.*, 2023, **144**, 114382.
31 S. Ahmad, S. Rabbani, U. Salma and S. A. Khan, *J. Fluoresc.*, 2025, **35**, 11825–11836.
32 B. Zhao, Y. Xu, Q. Deng, W. Kan, Y. Fang, L. Wang and Y. Gao, *Tetrahedron Lett.*, 2016, **57**, 953–958.
33 T. G. Pavita, F. Khoerunnisa, R. B. Taqriban, R. Adnan and A. A. Septevani, *Polym. Adv. Technol.*, 2025, **36**, e70372.
34 M. Z. Jonaghani, H. Zali-Boeini and H. Moradi, *Spectrochim. Acta, Part A*, 2019, **207**, 16–22.
35 Y. Du, H. Zhao, X. Peng, X. Zhou, X. Yang, Y. Li, M. Yan, Y. Cui and G. Sun, *J. Photochem. Photobiol., A*, 2023, **439**, 114604.
36 K. Tao, K. Imato and Y. Ooyama, *RSC Adv.*, 2025, **15**, 36165–36174.
37 K. Krishna and Y. Sangappa, *Inorg. Chem. Commun.*, 2025, **175**, 114138.
38 S. Priya, E. Karthikeyan, C. P. Reshmi, P. D. Raju, C. V. Suneesh, K. Sandeep and A. R. Ramesh, *RSC Adv.*, 2025, **15**, 50001–50009.